Loss of MiR-192 Initiates a Hyperglycolysis and Stemness Positive Feedback in Hepatocellular Carcinoma

Yuanzhuo Gu
Zhejiang University
Fubo Ji
Zhejiang University
Niya Liu
Zhejiang University
Yongzhi Zhao
Zhejiang University
Xiyang Wei
Zhejiang University
Shiyuan Hu
Zhejiang University
Wei Jia
Hong Kong Baptist University
Xin Wei Wang
National Cancer Institute
Anuradha Budhu
National Cancer Institute
Juling Ji
Nantong University
Bin Zhao
Zhejiang University
Stephanie Roessler
University Hospital Heidelberg
Xin Zheng
EZKIT L.L.C.
Junfang Ji (junfangji@zju.edu.cn)
Zhejiang University https://orcid.org/0000-0002-3071-6494

Research

Keywords: Hepatocellular carcinoma, Cancer stem cell, miR-192, Glycolysis, c-Myc

Posted Date: August 17th, 2020

DOI: https://doi.org/10.21203/rs.3.rs-56821/v1

Version of Record: A version of this preprint was published on November 30th, 2020. See the published version at https://doi.org/10.1186/s13046-020-01785-7.

Abstract

Background: Emerging studies revealed that cancer stem cells (CSCs) possessed peculiar metabolic properties, which however remained largely unknown in hepatocellular carcinoma (HCC). Genetic silencing of liver-abundant miR-192 was a key feature for multiple groups of CSC-positive primary HCCs. We thus aimed to investigate essential metabolic features of hepatic CSCs via using HCCs with miR-192 silencing as a model.

Methods: Data integration analyses of miR-192 with metabolome and mRNA transcriptome in HCC cohort 1 were performed to investigate miR-192 related metabolic features. Cellular and molecular assays were performed to examine whether and how miR-192 regulated the identified metabolic feature. Co-culture systems consisting of HCC and non-HCC cells were established to explore effects of the metabolomic property on stemness features in HCC cells via interacting with non-HCC cells.

Results: High expression of glycolysis-related metabolites and genes presented in HCCs with low miR-192 and CSC-positive HCCs in two independent HCC cohorts. miR-192 knock-out cells displayed CSC features and miR-192 loss led to an enhanced glycolytic phenotype via targeting three glycolysis regulators, i.e., Glut1, Pfkfb3, and c-Myc. Meanwhile, c-Myc suppressed miR-192 transcription, ensuring a low-miR-192/high-c-Myc loop to maintain hyperglycolysis. Moreover, over-produced lactic acid from hyperglycolytic HCC cells stimulated the Erk phosphorylation of co-cultured non-HCC cells partially via NDRG3 and MCT1, which in turn promoted cell malignancy and stemness of HCC cells.

Conclusions: In CSC-positive HCCs, miR-192 loss enhanced glycolysis via a c-Myc/miR-192/glycolysis regulators signal loop, allowing HCC cells to actively coordinate with their environment non-HCC cells for further increased stemness and malignancy.

Background

Abnormal cancer metabolism is one of the ten cancer hallmarks. Cancer stem cells (CSCs) are implicated in tumor initiation as well as recurrence, and rising attentions are drawing to CSC metabolism[1, 2]. Recent studies indicate that CSCs have different metabolic properties when compared to the tumor bulk. CSCs exhibit a distinct metabolic phenotype that includes low mitochondrial respiration, high glycolytic activity, and/or high fatty acid oxidation based on tumor types and CSC biomarkers as well as isolation methods. Exploiting metabolic vulnerability of CSCs may provide new effective cancer therapies to diminish recurrence and metastasis.

Multiple hepatic CSC biomarkers such as EpCAM, CD133, CD90, CD44, and CD24, have been used to enrich tumorigenic CSCs in primary hepatocellular carcinoma (HCC), the fourth-most lethal neoplasm worldwide[3-9]. Although gene signatures and regulatory pathways of CSC^{+}HCCs were thoroughly investigated, their metabolic properties remained largely unknown except of few recent studies. Three studies revealed a high glycolysis rate and a low oxygen consumption rate (OCR) in $CD133^{+}$ hepatic CSCs[10], the importance of fatty acid oxidation in $CD133^{+}$ CSCs[11], and increased lipid metabolites

associated with stearoyl-CoA-desaturase in EpCAM$^+$ HCCs[12]. In this case, it is feasible and essential to investigate the key metabolic features being shared among different CSC biomarker positive HCCs.

MiR-192-5p (miR-192) is the 2nd most abundant miRNA in the liver[13]. Its genetic silencing frequently occurs in many groups of hepatic CSC marker-positive HCCs such as EpCAM$^+$, CD90$^+$, CD133$^+$, CD44$^+$ and CD24$^+$HCCs, as well as pluripotency marker-positive HCCs. HCC cells with miR-192 loss displayed a highly invasive phenotype and essential CSC features partially via the p53/miR-192/PABPC4 pathway[13, 14]. Given these, investigating the key metabolic feature in HCCs with miR-192 loss might allow us to explore the essential metabolic properties of multiple different groups of CSC$^+$HCCs.

Methods

Omics dataset

A total of five datasets from two HCC cohorts with 548 cases were used. In Cohort 1, there were a total of 176 Asian HCC cases, among which all cases had miRNA transcriptome (GSE6857) and mRNA transcriptome (GSE14520) and 22 cases had available metabolomics data [12, 13, 15-18] (Fig. 1a). In Cohort 2, there were 372 HCC cases with different ethnicities. Their miRNA and mRNA sequencing data were downloaded from The Cancer Genome Atlas (TCGA) and available *TP53* mutation status and *MYC* amplification information in 240 HCC cases were collected from www.cbioportal.org/index.do.

Cell lines and miR-192 knockout HCC cells

Human liver cancer cell lines including HLF, HLE, Huh7 and HepG2 cells; human embryonic kidney HEK293T cells; human hepatic stellate cell (HSC) line LX2 cells; human hepatocyte line HL7702 cells; and human leukemic monocyte cell line THP1 (with macrophage activation) were used in this study as described before[13, 19]. HLF, HLE and HuH7 were originally from JCRB, whereas HepG2, 293T and THP1 were from ATCC, and LX2 and HL7702 were from Chinese Academy of Sciences (Shanghai, China).

MiR-192 knockout HCC cells were generated using the CRISPR/Cas9 system. Single-guide RNAs (sgRNAs) were designed via an online web tool (http://crispr.mit.edu) to target the precursor mir-192. The synthesized sequences were cloned into pSpCas9(BB)-2A-Puro (PX459) vector. After transfection, positive miR-192 knockout clones were screened. All sequences are listed in Supplementary Table S1.

Plasmids, siRNAs and cell treatments

Lentiviral constructs pre-hsa-miR-control (pmiR-control) and pre-hsa-miR-192-5p (pmiR-192) with GFP as well as miRzip-control and miRZip-192-5p (miRZip-192) were from SBI Biosciences and stored in our laboratory. pmiR-control with RFP (pmiR-ctrl/RFP) and pmiR-192 with RFP (pmiR-192/RFP) were constructed by replacing GFP with Ds-Red between the HindIII and NotI sites. Lentiviruses were packaged with plasmids psPAX2 and pMD2.G (Addgene) in 293T cells. For infection, 5 MOI of each lentivirus was used for all our studies.

pMiR-Report-control (Luc-Ctrl), pmiR-192 reporter (192-pos reporter), and miRZip-192 reporter (Zip192 reporter) were constructed before[13]. The miR-192 binding regions in the 3'UTR or coding region of *GLUT1*, *PFKPB3*, and *MYC* were inserted into the monoclonal sites (HindIII/SpeI) of the pMiR-Report plasmid to make the corresponding luciferase constructs. The pT3-EF1α-c-Myc vector was originally modified from pT3-EF1α for c-Myc overexpression[20]. pGL-miR-192-5p (pGL-192) promoters were constructed by inserting different lengths of the miR-192 promoter region to the monoclonal site (KpnI/XhoI) of pGL4.20-basic (Promega). *PFKFB3* siRNA, *GLUT*1 siRNA and negative control siRNA were purchased from RiboBio Co, Guangzhuo, China. *TP53* siRNA, *MYC* siRNA, *NDRG3* siRNA, and *MCT1* siRNA were purchased from GenePharma Co., Shanghai, China. Lipofectamine 2000 (Invitrogen) reagent and Rfect siRNA Transfection Reagent (BIO-TRAN) were used for the transfections of plasmids and siRNAs, respectively. The detailed information for all primers and sequences is listed in Supplementary Table S1.

Nutlin-3a was purchased from Selleck Chemicals and dissolved in DMSO. When indicated, HCC cells were treated for 24 hours with 10 μM of Nutlin-3a.

Extracellular acidification rate (ECAR) and oxygen consumption rate (OCR) assays

In the XF8 Extracellular Flux Analyzer (Seahorse Bioscience), the ECAR and OCR were measured using the Seahorse XF Glycolysis Stress Test Kit (Agilent Technologies) and Seahorse XF Cell Mito Stress Test Kit (Agilent Technologies), respectively. Experiments were performed according to the manufacturer's instructions. For the ECAR measurement, cells (1×10^4 cells/well) were plated in an XF8 cell-culture microplate for 12 hours and the culture medium was then replaced with XF assay medium. The ECAR was measured by the sequential addition of glucose, oligomycin, and 2-deoxyglucose (2DG) in an XF8 flux analyzer. For the OCR measurement, cells (1×10^4 cells/well) were plated in an XF8 cell-culture microplate for 12 hours and then culture medium was replaced with XF assay medium. The OCR was measured by sequential addition of oligomycin, FCCP, and antimycin A. Data were analyzed by Seahorse XF Wave software. The results were normalized to the cell number.

Co-culture system

Two types of co-culture systems were used. One was that HCC cells infected with corresponding RFP or GFP lentivirus were co-cultured with non-HCC cells. In this system, the results from cells labeled as Red or GFP were regarded as HCC cells. The other co-culture system was a chamber system using Polyester (PET) Membrane Tissue Culture Plate Insert with 0.4 μm pores (JET biofil) according to the manufacturer's protocol. Generally, non-HCC cells including LX2 or HL7702 were placed in the bottom layer of a 6-well plate while HCC cells were placed in the cell inserts of this 6-well plate. In addition, HCC cells were also co-cultured with THP1, a suspension cell line.

RNA isolation, quantitative real-time PCR, and Western blot

Total RNA was isolated using TRIzol (Invitrogen) following manufacturer's instructions, and 1 μg of total RNA was reverse transcribed into cDNA using PrimeScript™ RT Reagent Kit with gDNA Eraser (TaKaRa). Quantitative reverse transcription polymerase chain reaction (qRT-PCR) was performed with TB Green™ Premix EX Taq™ II (Tli RNaseH Plus) (TaKaRa). The expression of mature miRNAs was measured using TaqMan MiRNA Assays as described previously[17, 21, 22]. RNU6B was used as the reference gene for miRNAs, while 18S was the reference for measured mRNAs. Primers for *TACSTD1, CD133, CD90, CD44, CD24,* and *UGT2B7* were used as before[13]. Primer sequences for *GLUT1*, *HK2, PFKP, PFKFB3, ALDOA, ENO2, PKM2, LDHA, MCT4, MCT1, NDRG3* and *CYP1A2* are listed in Supplementary Table S1. The experiments were performed in triplicate.

For the Western blot assay, cells were lysed and processed as previously[17, 22]. The membranes with transferred protein extracts were incubated with the indicated primary antibodies and secondary antibodies conjugated to horseradish peroxidase for enhanced chemiluminescence detection of the signals (Amersham, Arlington Height, IL). The detailed information of all antibodies is listed in Supplementary Table S2.

Non-targeted metabolomics study

The non-targeted metabolomics was performed by Metabo-Profile Biotechnology (Shanghai) Co., Ltd. Metabolites identified and quantified from gas chromatography/time-of-flight mass spectrometry (GC/TOF-MS) data was performed in the workflow of ADAP-GC 2.0. Cell lysates and cell culture medium were collected from cells and used for metabolomics analysis. Each experiment was performed in triplicate.

2-NBDG uptake, glucose measurement and lactate measurement

Glucose uptake of HCC cells was quantified by flow cytometry using the fluorescent D-glucose derivate 2-(N-(7-nitrobenz-2-oxa-1,3-diazol-4-yl)amino)-2-deoxy-D-glucose (2-NBDG). A glucose measurement kit (Shanghai Rongsheng Biotech Co., Ltd.) was used to measure the glucose concentration in cell culture medium. Extracellular lactate production was measured using a lactate assay kit (Nanjing Jiancheng Bioengineering Institute). All these assays were performed according to the manufacturer's protocols.

Sphere formation assay, fluorescence-activated cell sorting (FACS) analysis

Single-cell suspensions of 1000 cells were seeded in 6-well Ultra-Low Attachment Microplates (Corning, Corning, NY) for spheroid assays. The number of spheroids was measured 12 days after seeding. For FACS analysis, cultured cells were trypsinized, washed, and resuspended in phosphate-buffered saline plus 0.5% bovine serum albumin. They were incubated with APC-conjugated antibodies on ice for 20 mins in the dark. Data were collected with a FACSCalibur flow cytometer (BD Biosciences) and analyzed using FlowJo software (Tree Star). The detailed information for all antibodies is listed in Supplementary Table S2.

Luciferase reporter assay

The pMiR-Report plasmids (with or without mature miR-192 binding sites) were transfected together with pRL-null vector containing Renilla luciferase. The Firefly and Renilla luciferase activities were measured 24 hours after transfection using Dual-Luciferase Reporter Assay (Promega, CA) with the luminometer. Each experiment was performed in triplicate and repeated at least three times.

To examine the promoter activity of miR-192, HCC cells (24-well plate) were transfected with 300 ng pT3-EF1α vector or pT3-EF1α-cMyc vector, or 50 nM siRNAs (negative control or *MYC* siRNAs) on the first day and then transfected with 300ng pGL-192 promoter constructs and 10 ng pRL-CMV on the next day. The Firefly and Renilla luciferase activities were then measured 24 hours after transfection.

Statistics

Spearman's rank correlation was performed to identify metabolites associated to miR-192. Student's t-test and Mann-Whitney rank test were used for statistical analysis of comparative data between groups. Two-way ANOVA was used to compare the glucose consumption, lactate production and cell viability of HCC cells at different time points. Hierarchical clustering analysis was performed by GENESIS software version 1.7.6 developed by Alexander Sturn (IBMT-TUG, Graz, Austria). Pearson correlation was used to identify genes correlated with miR-192. Kaplan–Meier survival analysis was used to compare patient survival based on prediction results using GraphPad Prism V7.0 (San Diego, CA), and the p-value was generated by the Cox–Mantel log-rank test. Gene set enrichment analysis (GSEA) in the Molecular Signatures Database was performed using GSEA V3.0. All p-values were 2-sided. A p-value of ≤ 0.05 was statistically significant.

Results

Glycolysis-related metabolites and genes were highly expressed in HCC cases with low miR-192 expression

To investigate the metabolic feature in HCCs with miR-192 silencing, we used HCC Cohort 1 with available metabolome and transcriptome data (Fig. 1a). An integration analysis of miR-192 with the global metabolome in tumor tissues from 22 HCC patients showed that 17 metabolites were significantly correlated with miR-192 (|r-value| >0.4, Fig. 1b, Supplementary Table S3). Among them, 7 metabolites presented |r-value| >0.5 and three of them were glycolysis-related metabolites, i.e., G6P, F6P, and NADPH. Meanwhile, 652 genes were significantly correlated with miR-192 with |r-value| >0.4, revealed by an integration analysis of miR-192 with mRNA transcriptome in tumor tissues from 176 HCC patients (Fig. 1c). KEGG pathway analysis using these genes displayed 13 enriched metabolomic features ($p<0.001$), among which three of them related to glycolysis and its related pathway. These results suggest an altered glycolytic feature in HCC cases with low miR-192 expression.

Available glycolysis-related metabolites and genes in our profiling data (Fig. 1d) were then compared between HCCs with high miR-192 levels (termed $HCC^{192High}$) and HCCs with low miR-192 levels (termed HCC^{192Low}), based on the miR-192 median cut-off in HCC tumors. Levels of G6P, F6P, and NADPH were significantly higher in tumors from HCC^{192Low} patients than $HCC^{192High}$ patients, while as a control there was no difference in their non-tumor tissues (Fig. 1e, Supplementary Fig. S1a). Consistently, many genes coding key enzymes in glycolysis such as *GLUT1, HK2, PFKFB3, PFKP, and PKM2* were significantly upregulated in HCC^{192Low} tumors compared to $HCC^{192High}$ tumors (Fig. 1e) but showed negligible alteration in their non-tumor tissues (Supplementary Fig. S1b). *MCT1* was used as a negative control due to its main role in lactate import, but not in glycolysis[23, 24]. All of these demonstrate a hyperglycolytic metabolic feature in HCC cases with low miR-192 level.

We further investigated the hyperglycolytic feature in CSC^+ HCC cases, i.e., cases with the top quartile expression of CSC biomarker as previously defined [13]. The hierarchical clustering analysis with glycolytic genes in Cohort 1 revealed two HCC subgroups presenting different expression levels of glycolytic genes. Consistently in HCC subgroup with high expression levels of glycolysis-related genes, miR-192 level was low while various groups of CSC^+ HCC cases were enriched (Fig. 1d). Statistical analysis also presented that glycolytic genes expressed significantly higher levels in various groups of CSC^+ HCCs than CSC^- HCCs, while this effect was not noticed from comparisons of their non-tumor tissues (Supplementary Fig. S1c-d). Comparable data were observed in Cohort 2 with 372 HCC patients that significantly high levels of glycolytic genes presented in $HCCs^{192Low}$ and in multiple groups of CSC^+HCCs (Supplementary Fig. S1e). Together, these data indicated that the hyperglycolytic feature presented in various groups of CSC^+HCCs with low level of miR-192.

HCC cells with miR-192 loss were hyperglycolytic.

We next investigated roles of miR-192 in regulating glycolysis. Lentivirus miRZip-192 was used to reduce miR-192 activity in Huh7 cells (Supplementary Fig. S2a), as we have done previously[13]. Huh7 cells with suppressed miR-192 by miRZip-192 exhibited the overall increased expression of glycolytic genes (Supplementary Fig. S2a), a distinctly increased ECAR and a reduced OCR (Fig. 1g). The extracellular acid produced by cells is derived from lactate produced by glycolysis and CO_2 produced during respiration. OCR is mainly representing mitochondrial respiration. Therefore, the increased ECAR in Huh7 cells with suppressed miR-192 was mainly due to lactate produced from glycolysis but not CO_2 from mitochondrial respiration. Consistently, overexpressed miR-192 in HLF and HLE cells generally reduced the expression levels of glycolytic genes (Supplementary Fig. S2b) and lowered the extracellular acid production from glycolysis as shown by a reduced ECAR but an increased OCR (Fig. 1h). These results demonstrate an important role of miR-192 in operating a Warburg-like effect in HCC cells.

To better elucidate the role of miR-192 in regulating glycolysis, we established two miR-192 knock-out (termed 192KO) human HCC cell lines and miR-192 was undetected in HLE-192KO and HLF-192KO cells (Fig. 2a). As a control, the expression of miR-194, 109 nucleotides away from mir-192, was not affected.

As we expected, HLF-192KO cells displayed significantly increased CSC features, such as increased populations of $CD44^+$, $CD24^+$ and $EpCAM^+$ CSCs (Fig. 2b, Supplementary Fig. S2c); increased mRNA levels of multiple CSC biomarkers and reduced expression of a differentiation-related gene *CYP1A2* (Supplementary Fig. S2d); and enlarged and more spheroid formation (Supplementary Fig. S2e). HLE-192KO cells displayed the increased CSC features at a moderate level (Fig. 2b, Supplementary Fig. S2c-d). Consistently, these two 192KO lines also showed the hyperglycolytic features. Many key enzyme proteins in glycolysis pathway were more highly expressed in 192KO cells than in wild-type cells (Fig. 2c). Both 192KO lines also exhibited increased ECARs but decreased OCRs (Fig. 2d), indicating that miR-192 loss largely increased the glycolysis-related extracellular acidification.

Furthermore, overexpressed miR-192 in HLF-192KO cells significantly reduced the CSC features and the lactate accumulation in culture medium by miR-192 loss (Fig. 2e). As a control, intracellular lactate remained no change. Meanwhile, following culture time, lactate accumulation in the medium was gradually increased and significantly higher in both HLF-192KO cells in HLE-192KO cells compared with that in their corresponding wild-type cells, which was lowered by overexpressed miR-192 (Fig. 2f). It could also be visualized via the orange/yellow medium of 192KO cells (referring to a lower pH value) vs. the pink medium of wild-type cells at 72 hours after seeding. Consistent data were obtained in detection of metabolites using non-targeted metabolomics in HLF cells with different expression of miR-192-5p in both internal cells and culture medium (Supplementary Fig S2f). Together, miR-192 loss in HCC cells led to a hyperglycolytic feature.

HCC cells with miR-192 loss had high glucose consumption

We further examined that glucose consumption among HCC cells with different levels of miR-192 and between HCC cells and their surrounding cells in the liver. As shown in Fig. 3a, both HLF-192KO and HLE-192KO cells exhibited significantly higher glucose consumption than HCC cells overexpressing miR-192. In Huh7 cells, suppressing miR-192 by miRZip-192 increased their glucose usage (Supplementary Fig. S3a). Consistently, 192KO HCC cells were more sensitive after exposure to 2-DG, a glucose analog, as shown by the significantly reduced cell viability compared to HCC cells with miR-192 expression (Fig. 3b). Comparable data were obtained in HuH7 cells (Supplementary Fig. S3b).

In co-culture systems of HCC cells with environmental non-HCC cells including LX2, HL7702, and THP1, we further compared the glucose uptake of HCC cells with different miR-192 level and non-HCC cells via 2-NBDG uptake assay. HLF HCC cells infected with pmiR-ctrl/RFP and pmiR-192/RFP lentiviruses were used, which showed that red fluorescent labeling efficiency is nearly 100% (Supplementary Fig. S3c). In this system, with/without co-culturing with other cells, HLF-192KO cells consistently showed higher 2-NBDG uptakes than the wild-type cells (Fig. 3c-d). In contrast, LX2 and HL7702 co-cultured with HLF-192KO cells presented lower 2-NBDG uptakes compared to those co-cultured with HLF-WT cells (Fig. 3d). Moreover, forced-expression of miR-192 in HLF-192KO cells reduced the 2-NBDG uptake in HLF cells but increased the 2-NBDG uptake in LX2 and HL7702 cells in the co-culture system. The 2-NBDG uptake alteration was not noticed in THP1 from our co-culture system (Fig. 3d, Supplementary Fig. S3d). Similar

data were noticed in HLE cells as well as in the co-culture assay of HLE with LX2 and HL7702 cells (Supplementary Fig. S3e-f). These results demonstrate that HCC cells with loss of miR-192 actively utilize glucose from their environment to ensure a hyperglycolysis status.

Three important glycolytic regulators were miR-192 *bona fide* targets and also contributed to stemness features of HCC cells

To investigate the molecular mechanisms of miR-192 regulating glycolysis flow, we assessed genes negatively correlated with miR-192 in 176 HCC cases ($r<-0.3$) and significantly up-regulated in HCC^{192Low} tumors than in $HCC^{192High}$ tumors (log_2fold >0.2, $p<0.01$). Among these 554 genes, two main gene-groups were noticed. One group contained genes related to cell migration as we reported before[13]. The other group included eight glycolysis-related genes (Fig. 4a) and three of them (*GLUT1, HK2*, and *PKM2*) were reported as targets of c-Myc, a key regulator in glycolysis[25, 26].

TargetScan program and manual miRNA target prediction identified four of these glycolytic genes containing miR-192 binding sites in their 3'UTR and/or coding regions (Fig. 4a). They were *PFKFB3, GLUT1, MCT4*, and *MYC*. In HLF and HLE cells, overexpressed miR-192 reduced the protein levels of Pfkfb3, Glut1, and c-Myc, but not that of Mct4 (Fig. 4b). Further, the predicted miR-192 binding regions in these three genes were cloned into a luciferase reporter and forced expression of miR-192 reduced the luciferase activities when the wild-type sequences for *PFKFB3* and *GLUT1* as well as the #2 binding site of *MYC* were present (Fig. 4c). These effects were significantly reduced when the corresponding miR-192 binding sites were mutated. Moreover, silencing Pfkfb3, Glut1, or c-Myc using two different siRNAs reduced ECAR in both HLF-WT and HLF-192KO cells (Fig. 4d, Supplementary Fig. S4a). In HLF-192KO cells, silencing Pfkfb3, Glut1 or c-Myc notably reduced the ECAR rate to a level similar to that of HLF-WT cells with silencing of these genes. Comparable data were also noticed in HCC patients from Cohorts 1 and 2 that *PFKFB3*, *GLUT1*, and *MYC* presented higher levels in HCC^{192Low} tumors compared to $HCC^{192High}$ tumors (Supplementary Fig. S4b-c). These results indicate that Pfkfb3, Glut1, and c-Myc are miR-192 targets and involved in the hyperglycolysis caused by miR-192 loss.

Pfkfb3, Glut1, and c-Myc were reported to maintain stemness features in cancers at certain levels [27-30]. Consistently, si-*PFKFB3,* si-*GLUT1* or double knockdown led to reduced levels of four CSC biomarkers, i.e., *CD44*, *CD24*, *EpCAM* and *CD90*, as determined by RT-qPCR (Fig. 4e). FACS analysis also showed that si-*PFKFB3* and *GLUT1* reduced the populations of $CD44^+$ and $CD24^+$ CSCs (Fig. 4f). Meanwhile, si-*MYC* seemed to only reduce $CD44^+$ CSCs moderately, but not $CD24^+$ CSC populations (Supplementary Fig. S4d). Together, these data demonstrate that three glycolytic regulators, Pfkfb3, Glut1 and c-Myc were *bona fide* targets of miR-192, and they contributed to both hyper-glycolysis and CSC features of HCCs caused by loss of miR-192 to different extents.

c-Myc suppressed miR-192 transcription, ensuring a positive feedback of high c-Myc/low miR-192 in hyperglycolytic CSC^+HCCs

In our previous miRNA profiles of tumors and non-tumors from a hydrodynamic injection HCC FVB mouse model[20], miR-192 expression was significantly reduced in c-Myc-induced HCCs (Fig. 5a). Further, in a hydrodynamic injection HCC ICR mouse model, miR-192 level was also reduced >100 times in c-Myc induced HCCs but not much reduced in Ras-induced HCCs than that in the corresponding non-HCC liver tissues. In four different HCC cell lines, si-*MYC* led to an increased expression of miR-192, while forced expression of c-Myc reduced the level of miR-192 (Fig. 5b). These indicate that c-Myc might regulate miR-192 transcription.

Consistently, among four different lengths of mir-192 promoter regions, the -266 nt to +186 nt region showed the strongest promoter activity (Fig. 5c) and the mir-192 promoter activity (-266 nt to +186 nt) was reduced by exogenous c-Myc, while enhanced by si-*MYC* (Fig. 5d). Wild-type p53 could bind to the mir-192 promoter region and induce its expression[13, 31]. Consistently, in HepG2 cells with wild-type *TP53,* the expression of miR-192 was induced by p53 via exposure to Nutlin-3a (an MDM2 antagonist to stabilize p53) and reduced by silencing of p53 (Fig. 5e, Supplementary Fig. S5a-b). Meanwhile, over-expressed c-Myc significantly suppressed miR-192 expression in HCC cells with either activated p53 or silenced p53, indicating that c-Myc-mediated miR-192 down-regulation was independent on p53.

Comparable data were noticed in HCC patients. In both HCC cohorts, hierarchical clustering analysis revealed two subgroups with distinct c-Myc activation status based on 76 c-Myc target genes from the online Human MYC Targets Profiler (Supplementary Fig. S5c-d). In Cohort 1, miR-192 expression in the c-Myc activation subgroup was significantly lower than that in c-Myc non-activation subgroup (Fig. 5f). In Cohort 2, mir-192 expression was always significantly lower in each c-Myc activation subgroup than in the corresponding non-activation subgroup, which was independent on statuses of TP53 and mir-192 promoter methylation (Fig. 5f. In addition, different groups of CSC^+HCCs consistently presented a low level of miR-192, a high level of c-Myc activation and high frequency of *MYC* amplification (Supplementary Fig. S6). Together, c-Myc suppressed miR-192 transcription, which led to a positive feedback of high c-Myc/low miR-192 in CSC^+HCC cells with glycolytic feature.

Overproduced lactate from CSC^+HCCs activated the Erk pathway in HCC environmental cells, and this effect further increased HCC cell stemness and malignancy features

As the end product of glycolysis, the continuously produced lactate from hyperglycolytic miR-192-loss HCC cells might affect their environment and contribute to HCC malignancy. The transport of lactate across the plasma membrane is mainly catalyzed by MCT1 and MCT4, with MCT1 typically involved in the import while MCT4 involved in export of lactate[23, 24]. In HCC patients, the expression ratio of *MCT1 vs. MCT4* presented no difference between tumor and non-tumor tissues of Cohort 1 but was significantly higher in non-tumor tissues than tumor tissues of Cohort 2 (Supplementary Fig. S7a), indicating the possibility of lactate uptake by tumor environmental cells. Lee et al reported that lactate could stabilize the NDRG3, which in turn activated the Erk pathway to promote cell malignancy[32]. Consistently, lactate treatment stimulated Erk phosphorylation noticeably in HCC environmental cells, i.e., LX2 and THP1 and HL7702 cells (Fig. 6a).

In a chamber co-culture system, pErk level was increased in LX2 and THP1 cells when they were co-cultured with HLF-192KO cells compared to when co-culturing with HLF-WT (Fig. 6b). Moreover, pErk was further reduced in LX2 and THP1 when exposed to HLF-192KO cells with miR-192 overexpression (Fig. 6b). Similar results were observed from co-cultured LX2 and THP1 cells with HLE cells (Supplementary Fig. S7b). However, pErk did not seem to be altered in HL7702 cells in this co-culture system. Thus, HCC cells with miR-192 loss could actively affect certain group of cells in their environment via an increased lactate production and secretion.

Fig. 6c-e showed that the lactate-induced pErk in HCC environmental cells partially relied on NDRG3 and MCT1. LX2 and THP1 cells expressed relatively high levels of *MCT1* and *NDRG3* (Fig. 6c). Silencing NDRG3 or MCT1 in LX2 and THP1 cells reduced the level of lactate-induced pErk (Fig. 6d-e). Low expression levels of MCT1 and NDRG3 in HL7702 cells were consistent with its minor response to lactate (data not shown).

We then explored the effects of an altered lactate/MCT1/NDRG3/pErk axis in LX2 or THP1 cells on the malignancy features of HCC cells. HLF-192KO/RFP cells were co-cultured with LX2 cells pre-transfected with si-Ctrl, or si-*NDRG3*, or si-*MCT1* (termed $LX2^{si\text{-}Ctrl}$, $LX2^{si\text{-}NDRG3}$, and $LX2^{si\text{-}MCT1}$, respectively). Wound-healing assay under red fluorescence showed that cell migration of HLF-192KO cells was slower in co-culture with $LX2^{si\text{-}NDRG3}$ or $LX2^{si\text{-}MCT1}$ than in co-culture with $LX2^{si\text{-}Ctrl}$ (Fig. 7a). Consistent data were observed in HLF-192KO cells co-cultured with THP1 (Fig. 7a). Moreover, spheroid assays of HLF-192KO cells were performed with different conditioned medium. The number of spheroids of HLF-192KO cells was significantly lower under exposure to conditioned medium from co-culture of HLF-192KO with $LX2^{si\text{-}NDRG3}$ or $LX2^{si\text{-}MCT1}$ than from co-culture of HLF-192KO with $LX2^{si\text{-}Ctrl}$ (Fig. 7b). $CD44^+$ and $CD24^+$ HLF-192KO populations were also significantly reduced when they were co-cultured with $LX2^{si\text{-}NDRG3}$ or $LX2^{si\text{-}MCT1}$ (Fig. 7c). As a control, HLF-192KO with overexpressed miR-192 did not exhibit much alteration on migration, spheroid formation and CSC populations when co-culturing with different LX2 cells (Fig. 7a-c). Therefore, in co-culture system, blocking a lactate/Erk pathway in HCC environmental cells suppressed the malignancy and stemness features of HCC cells.

In both HCC cohorts, patients were divided into four groups based on miR-192 expression in their tumor (HCC^{192Low} and $HCC^{192High}$, medium cut-off) and levels of NDRG3 and MCT1 in non-tumors ($NT^{High\_NDRG3\ or\ MCT1}$ and $NT^{Low\_NDRG3\ and\ MCT1}$, medium cut-offs). There was no expressional difference of NDRG3 or MCT1 in non-tumors between HCC^{192Low} and $HCC^{192High}$ patients (Fig. 7d, Supplementary Fig. S7C). In Cohort 1, patients with $HCC^{192High}$ $NT^{Low\_NDRG3\ and\ MCT1}$ had the best prognosis, as shown by a prolonged time to recurrence and overall survival. In HCC^{192Low} subgroup, patients with $NT^{High\_NDRG3\ or\ MCT1}$ had worse prognosis compared to patients with $NT^{Low\_NDRG3\ or\ MCT1}$ (Fig. 7e). Similar but less significant data were obtained from Cohort 2, which might be due to the limited number of patients (n=49) with available non-tumor mRNA reading (Supplementary Fig. S7d). GSEA analysis in HCC^{192Low} patients revealed that several stem cell related gene-sets were enriched in patients with $NT^{High\_NDRG3\ or\ MCT1}$ those with $NT^{Low\_NDRG3\ or\ MCT1}$ (Supplementary Fig. S8). Together, when HCC cells with miR-192 loss

surrounded by environmental cells with high MCT1 or NDRG3 expression, they presented a highly malignant feature.

Discussion

HCC is one of the most malignant cancers worldwide. With the trend of decreasing incidence for many cancers, the incidence of HCC is still rising in both developing and developed countries[33]. CSCs are thought to be responsible for tumorigenesis as well as tumor metastasis and arising attentions have been drawn to CSC metabolism with the hope of eliminating cancer[1, 2]. In this study, we aimed to understand essential metabolic features of hepatic CSCs.

MiR-192 is functionally important in suppressing the stemness and malignancy features of HCC cells, and its genetic silencing frequently occurs in multiple different groups of CSC^+ HCCs[13]. Here, we revealed that the miR-192 loss drove HCC cells to the hyperglycolytic metabolism status via a c-Myc/miR-192/glycolytic genes positive feedback pathway, which also contributed to the increased CSC features of HCC cells. Multiple groups of CSC^+HCCs all presented a hyperglycolytic signature, high level of c-Myc and low miR-192. Mechanistically, loss of miR-192 led to increased expression of its target genes, i.e., Pfkfb3, Glut1 and c-Myc, which facilitated the Warburg effect being favored by cellular growth and stemness. Moreover, c-Myc also directly suppressed miR-192 expression, ensuring a positive feedback to drive hyperglycolytic features in CSC^+HCCs. In addition, targeting Pfkfb3, Glut1 and c-Myc could also reduce hepatic CSC populations. However, it remained unclear whether liver cells gained their CSC features and hyperglycolysis features at the same time or if one is the consequence of the other. The efforts to answer these questions will further improve our understanding of HCC initiation and even open a new area to prevent HCC tumor initiation or metastasis.

The non-HCC cells surrounding the HCC bulk tumor include HSCs, macrophages and non-HCC liver cells, and are believed to actively interact with HCC tumors as well as affect their malignancy status. Here, we identified that HCC environmental cells with high levels of NDRG3 and/or MCT1 facilitated a more malignant phenotype of HCC with miR-192 loss. Hyperglycolytic miR-192 silencing cells nourished the surrounding cells with overproduced lactate, which stimulated the pErk pathway in the surrounding non-HCC cells via NDRG3/MCT1. This activated pathway in turn promoted the HCC malignancy and stemness. Thus, the idea of HCC precision medicine would need more input on the interaction of the tumor and its environment to offer a better solution of cancer therapy. In our study, it remained undiscovered how MCT1/NDRG3 expression was regulated, whether there are any other mechanisms involved in interacting with HCC tumors, and how the pErk pathway in non-HCC cells promoted HCC malignancy. It is certainly interesting to perform an in-depth study on cytokines or exosomes being produced by non-HCC cells through the lactate/Erk axis, and their roles in promoting the malignancy of tumor cells. Future systematic studies will be needed on the microenvironment of HCCs with different levels of miR-192 in tumors.

Conclusions

Taken together, loss of miR-192 ensured hyperglycolysis and stemness features in CSC^{+}HCC cells through a c-Myc/miR-192/glycolysis genes positive feedback circuit. Moreover, HCC cells with miR-192 loss could also actively interact with their environment for a more aggressive and stemness-related feature via the over-produced lactic acid by HCC cells and consequently activating a lactate/MCT1/NDRG3/pErk pathway in their environmental cells (Fig. 7f).

Abbreviations

Cancer stem cell, CSC; Extracellular acidification rate, ECAR; Fluorescence-activated cell sorting, FACS; Gas chromatography/time-of-flight mass spectrometry, GC/TOF-MS; Gene Set Enrichment Analysis, GSEA; Hepatocellular carcinoma, HCC; Hepatic stellate cell, HSC; Oxygen consumption rate, OCR; Quantitative reverse transcription polymerase chain reaction, qRT-PCR; Single-guide RNAs, sgRNAs; The Cancer Genome Atlas, TCGA; 2-deoxyglucose, 2-DG; 2-(N-(7-nitrobenz-2-oxa-1,3-diazol-4-yl)amino)-2-deoxy-D-glucose, 2-NBDG.

Declarations

Ethics approval and consent to participate

Not applicable

Consent for publication

Not applicable

Availability of data and materials

miRNA transcriptome in HCC cohort 1, GSE6857; mRNA transcriptome in HCC cohort 1, GSE14520; metabolomics data in HCC cohort 1 were referenced in Ref 12. miRNA sequencing and mRNA sequencing data were downloaded from TCGA. TP53 mutation status and MYC amplification information in HCC cohort 2 were collected from www.cbioportal.org/index.do.

Competing interests

The authors have no conflicts of interest with the material presented in this manuscript.

Funding

This work was supported by National Key R&D Program of China (2018YFA0800504) (J. Ji), National Natural Science Foundation of China (No.81672905 and 81874054) (J. Ji), the Fundamental Research Funds for the Central Universities in China (J. Ji), and the Thousand Young Talents Plan of China (J. Ji).

X.W.W. and A.B. were supported by the intramural program of the Center for Cancer Research, the U.S. National Cancer Institute.

Authors' contributions

Conception and design: Y. Gu., and J. Ji.; Development of methodology: Y. Gu., F. Ji., N. Liu., J. Ji.; Acquisition of data: Y. Gu., N. Liu., Y. Zhao., S. Hu., J. Ji.; Analysis and interpretation of data (e.g., statistical analysis, biostatistics, computational analysis): Y. Gu., F. Ji., X. Wei., J. Ji.; Writing, review, and/or revision of the manuscript: Y. Gu., X. Wang., A. Budhu., S. Roessler., J. Ji.; Administrative, technical, or material support: X. Zheng., B. Zhao., X. Wang., A. Budhu., W. Jia., J. Ji.; Study supervision: J. Ji.

Acknowledgments

We thank Dr. Chaohui Yu for the HL7702 cell line, Dr. Long Zhang for the THP1 cell line, Dr. Xing Guo for PX459 plasmid and Dr. Hai Song for the anti-pErk and anti-Erk antibodies. The authors thank our core facility at Life Sciences Institute for their support on FACS analysis and measurement using Sea Horse XF Analyzers.

References

1. Gupta PB, Chaffer CL, Weinberg RA: Cancer stem cells: mirage or reality? Nat Med. 2009;15:1010-2.
2. Oikawa T: Cancer Stem cells and their cellular origins in primary liver and biliary tract cancers. Hepatology. 2016;64:645-51.
3. Lee TK, Castilho A, Cheung VC, Tang KH, Ma S, Ng IO: CD24(+) liver tumor-initiating cells drive self-renewal and tumor initiation through STAT3-mediated NANOG regulation. Cell Stem Cell. 2011;9:50-63.
4. Yamashita T, Ji J, Budhu A, Forgues M, Yang W, Wang HY *et al*: EpCAM-positive hepatocellular carcinoma cells are tumor-initiating cells with stem/progenitor cell features. Gastroenterology. 2009;136:1012-24.
5. Yang ZF, Ho DW, Ng MN, Lau CK, Yu WC, Ngai P *et al*: Significance of CD90+ cancer stem cells in human liver cancer. Cancer Cell. 2008;13:153-66.
6. Ma S, Tang KH, Chan YP, Lee TK, Kwan PS, Castilho A *et al*: miR-130b Promotes CD133(+) liver tumor-initiating cell growth and self-renewal via tumor protein 53-induced nuclear protein 1. Cell Stem Cell. 2010;7:694-707.
7. Ma S, Chan KW, Hu L, Lee TK, Wo JY, Ng IO *et al*: Identification and characterization of tumorigenic liver cancer stem/progenitor cells. Gastroenterology. 2007;132:2542-56.
8. Suetsugu A, Nagaki M, Aoki H, Motohashi T, Kunisada T, Moriwaki H: Characterization of CD133+ hepatocellular carcinoma cells as cancer stem/progenitor cells. Biochem Biophys Res Commun. 2006;351:820-4.

9. Zhu Z, Hao X, Yan M, Yao M, Ge C, Gu J *et al*: Cancer stem/progenitor cells are highly enriched in CD133+CD44+ population in hepatocellular carcinoma. Int J Cancer. 2010;126:2067-78.
10. Song K, Kwon H, Han C, Zhang J, Dash S, Lim K *et al*: Active glycolytic metabolism in CD133(+) hepatocellular cancer stem cells: regulation by MIR-122. Oncotarget. 2015;6:40822-35.
11. Chen CL, Uthaya Kumar DB, Punj V, Xu J, Sher L, Tahara SM *et al*: NANOG Metabolically Reprograms Tumor-Initiating Stem-like Cells through Tumorigenic Changes in Oxidative Phosphorylation and Fatty Acid Metabolism. Cell Metab. 2016;23:206-19.
12. Budhu A, Roessler S, Zhao X, Yu Z, Forgues M, Ji J *et al*: Integrated metabolite and gene expression profiles identify lipid biomarkers associated with progression of hepatocellular carcinoma and patient outcomes. Gastroenterology. 2013;144:1066-75 e1.
13. Gu Y, Wei X, Sun Y, Gao H, Zheng X, Wong LL *et al*: miR-192-5p Silencing by Genetic Aberrations Is a Key Event in Hepatocellular Carcinomas with Cancer Stem Cell Features. Cancer Res. 2019;79:941-53.
14. Lian J, Jing Y, Dong Q, Huan L, Chen D, Bao C *et al*: miR-192, a prognostic indicator, targets the SLC39A6/SNAIL pathway to reduce tumor metastasis in human hepatocellular carcinoma. Oncotarget. 2016;7:2672-83.
15. Budhu A, Jia HL, Forgues M, Liu CG, Goldstein D, Lam A *et al*: Identification of metastasis-related microRNAs in hepatocellular carcinoma. Hepatology. 2008;47:897-907.
16. Ji J, Shi J, Budhu A, Yu Z, Forgues M, Roessler S *et al*: MicroRNA expression, survival, and response to interferon in liver cancer. N Engl J Med. 2009;361:1437-47.
17. Ji J, Yamashita T, Budhu A, Forgues M, Jia HL, Li C *et al*: Identification of microRNA-181 by genome-wide screening as a critical player in EpCAM-positive hepatic cancer stem cells. Hepatology. 2009;50:472-80.
18. Roessler S, Long EL, Budhu A, Chen Y, Zhao X, Ji J *et al*: Integrative genomic identification of genes on 8p associated with hepatocellular carcinoma progression and patient survival. Gastroenterology. 2012;142:957-66 e12.
19. Sun Y, Ji F, Kumar MR, Zheng X, Xiao Y, Liu N *et al*: Transcriptome integration analysis in hepatocellular carcinoma reveals discordant intronic miRNA-host gene pairs in expression. Int J Biol Sci. 2017;13:1438-49.
20. Tao J, Ji J, Li X, Ding N, Wu H, Liu Y *et al*: Distinct anti-oncogenic effect of various microRNAs in different mouse models of liver cancer. Oncotarget. 2015;6:6977-88.
21. Ji J, Zhao L, Budhu A, Forgues M, Jia HL, Qin LX *et al*: Let-7g targets collagen type I alpha2 and inhibits cell migration in hepatocellular carcinoma. J Hepatol. 2010;52:690-7.
22. Ji J, Zheng X, Forgues M, Yamashita T, Wauthier EL, Reid LM *et al*: Identification of microRNAs specific for epithelial cell adhesion molecule-positive tumor cells in hepatocellular carcinoma. Hepatology. 2015;62:829-40.
23. Dimmer KS, Friedrich B, Lang F, Deitmer JW, Broer S: The low-affinity monocarboxylate transporter MCT4 is adapted to the export of lactate in highly glycolytic cells. Biochem J. 2000;350 Pt 1:219-27.

24. Doherty JR, Cleveland JL: Targeting lactate metabolism for cancer therapeutics. J Clin Invest. 2013;123:3685-92.
25. Sabnis HS, Somasagara RR, Bunting KD: Targeting MYC Dependence by Metabolic Inhibitors in Cancer. Genes (Basel). 2017;8.
26. Stine ZE, Walton ZE, Altman BJ, Hsieh AL, Dang CV: MYC, Metabolism, and Cancer. Cancer Discov. 2015;5:1024-39.
27. Li HM, Yang JG, Liu ZJ, Wang WM, Yu ZL, Ren JG *et al*: Blockage of glycolysis by targeting PFKFB3 suppresses tumor growth and metastasis in head and neck squamous cell carcinoma. J Exp Clin Cancer Res. 2017;36:7.
28. Shibuya K, Okada M, Suzuki S, Seino M, Seino S, Takeda H *et al*: Targeting the facilitative glucose transporter GLUT1 inhibits the self-renewal and tumor-initiating capacity of cancer stem cells. Oncotarget. 2015;6:651-61.
29. Zhang HL, Wang MD, Zhou X, Qin CJ, Fu GB, Tang L *et al*: Blocking preferential glucose uptake sensitizes liver tumor-initiating cells to glucose restriction and sorafenib treatment. Cancer Lett. 2017;388:1-11.
30. Akita H, Marquardt JU, Durkin ME, Kitade M, Seo D, Conner EA *et al*: MYC activates stem-like cell potential in hepatocarcinoma by a p53-dependent mechanism. Cancer Res. 2014;74:5903-13.
31. Pichiorri F, Suh SS, Rocci A, De Luca L, Taccioli C, Santhanam R *et al*: Downregulation of p53-inducible microRNAs 192, 194, and 215 impairs the p53/MDM2 autoregulatory loop in multiple myeloma development. Cancer Cell. 2010;18:367-81.
32. Lee DC, Sohn HA, Park ZY, Oh S, Kang YK, Lee KM *et al*: A lactate-induced response to hypoxia. Cell. 2015;161:595-609.
33. Bray F, Ferlay J, Soerjomataram I, Siegel RL, Torre LA, Jemal A: Global cancer statistics 2018: GLOBOCAN estimates of incidence and mortality worldwide for 36 cancers in 185 countries. CA Cancer J Clin. 2018;68:394-424.

Figures

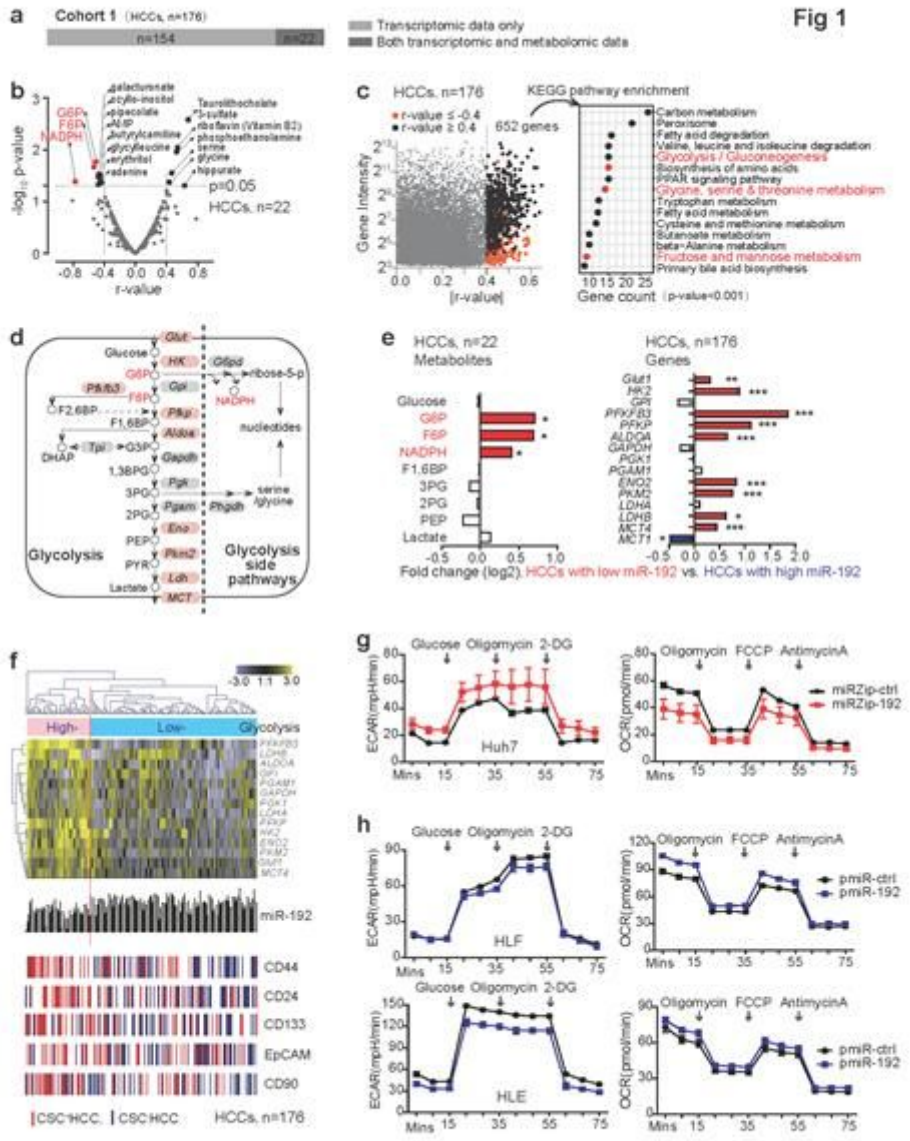

Figure 1

In HCCs, high expression of glycolysis-related metabolites and genes was associated with low miR-192 level. a. Available omics dataset in cohort 1 (n=176). b. Spearman correlation was performed between miR-192 and metabolome in 22 HCC cases of HCC Cohort 1. 17 metabolites were significantly correlated with miR-192 with |r-value| >0.4 ($p<0.05$). c. 652 genes significantly correlated with miR-192 (Pearson correlation, |r-value| >0.4) in cohort 1 were used for KEGG pathway enrichment analysis. d. Major metabolites and genes in glycolysis and glycolysis side pathways. e. Log2 ratios of glycolysis-related metabolites and genes in HCC192Low vs. HCC192High HCCs of Cohort 1. f. Hierarchical clustering analysis with glycolysis-related genes in cohort 1. Red bar and green bar represent CSC biomarker positive and negative HCC cases, respectively. miR-192 expression levels were also shown. g. ECAR and

OCR measurement in Huh7 cells infected with lentivirus miRZip-ctrl or miRZip-192. h. ECAR and OCR measurement in HLF and HLE cells infected with lentivirus pmiR-ctrl or pmiR-192.

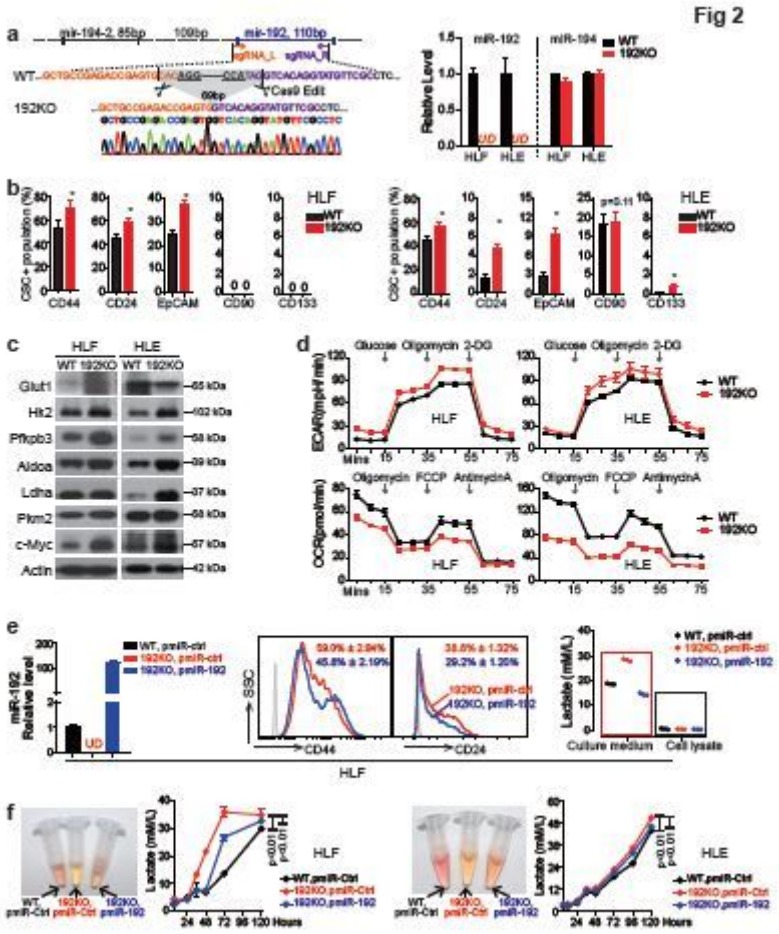

Figure 2

MiR-192 knock-out human HCC cell lines presented the increased CSC features and were highly glycolytic. a. Schematic structure of miR-192 wild-type (WT) and knock-out (KO) by CRISPR/Cas9 system. The knock-out of miR-192 DNA fragment was assessed by Sanger sequencing. Levels of miR-192 and miR-194-5p was measured by RT-qPCR. b. Quantitative data of FACS analysis using APC-conjugated antibodies against different CSC biomarkers in 192KO lines and WT lines from HLF and HLE cells. c. Western blot of glycolytic enzymes using 192KO lines and WT lines from HLF and HLE cells. d. ECAR and OCR were measured in 192KO lines and WT lines from HLF and HLE cells. e. RT-qPCR analysis of miR-192, FACS analysis of CD24+ and CD44+ populations, and lactate using Lactate assay kit in HLF cells with different levels of miR-192. f. Measurement of lactate in cultured medium at different time points from HLF and HLE cells. Representative images for color change of the corresponding cultured medium at 72hours after seeding were shown.

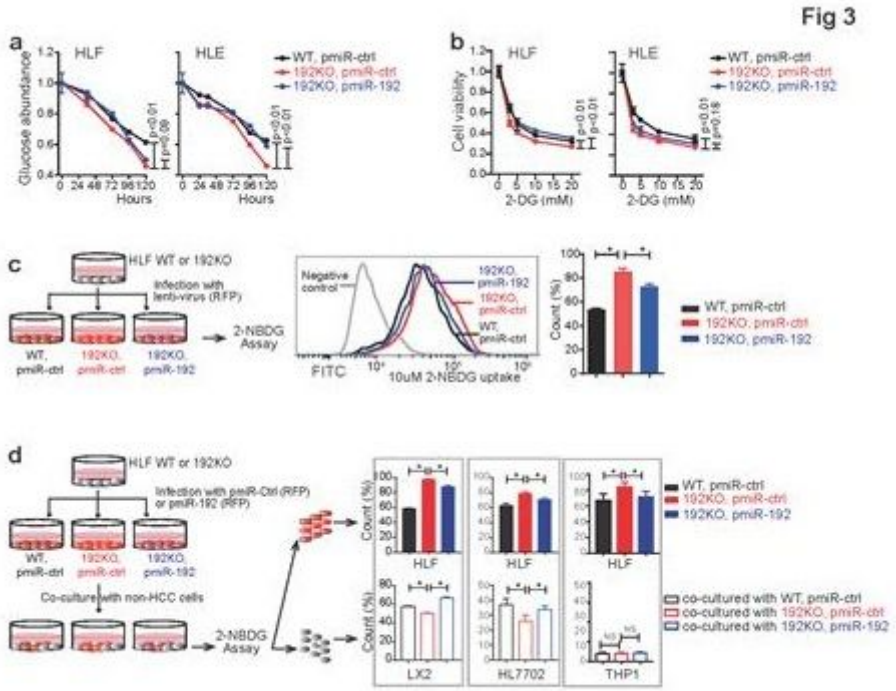

Figure 3

MiR-192 KO cells consumed more glucose from the environment. a. Glucose concentration in culture medium from WT and 192KO lines of HLE and HLF cells infected with lentivirus pmiR-Ctrl or pmiR-192. b. Cell viability of WT and 192KO lines for HLE and HLF cells infected with lentivirus pmiR-Ctrl or pmiR-192 and exposed to different doses of 2-DG. c. 2-NBDG uptake by FACS analysis of HLF-WT and -192KO cells infected with lentivirus pmiR-Ctrl (RFP) or pmiR-192 (RFP). d. 2-NBDG uptake by FACS analysis for all cells in co-culture system. HLF cells were infected with lentivirus pmiR-Ctrl (RFP) or pmiR-192 (RFP) and co-cultured with LX2, HL7702 or THP1 cells. Two-way ANOVA analysis was performed for (a, b) and student t-test was performed for (c,d). *, $p<0.05$.

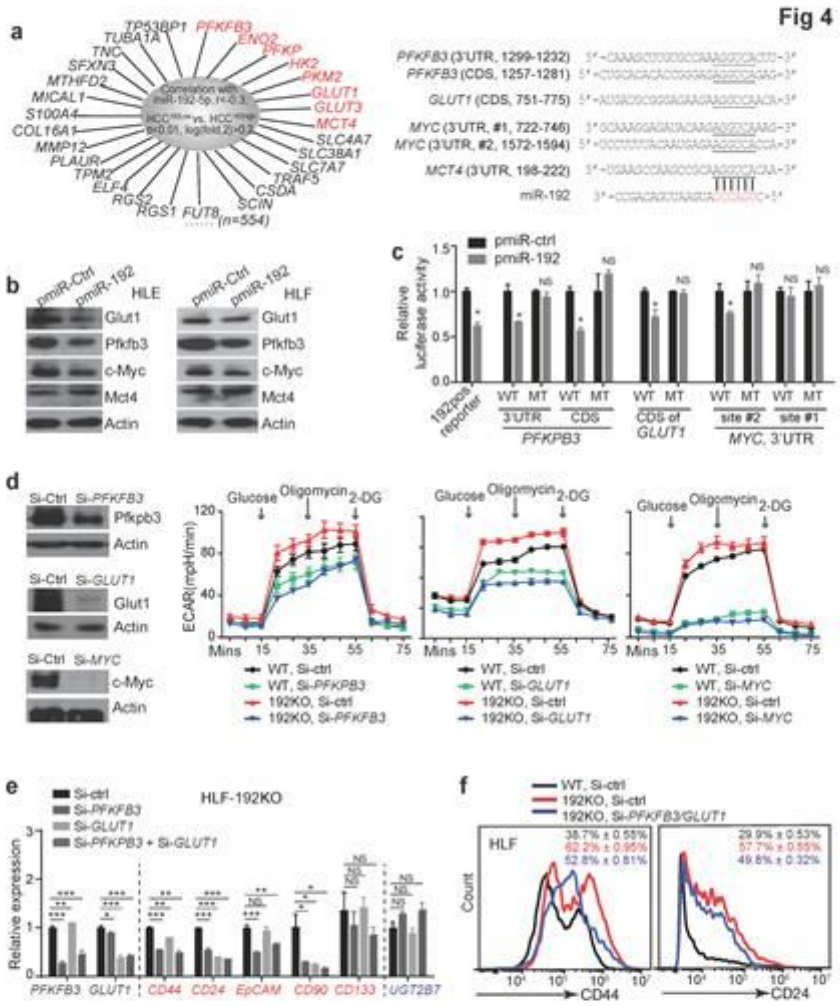

Figure 4

Several key genes in glycolysis pathway were miR-192 targets. a. Genes negatively correlated with miR-192 (r<-0.3) and significantly altered in HCC192Low vs. HCC192High and predicted miR-192 binding sites in 3'-UTR or coding regions (CDS) of human PFKFB3, GLUT1, MYC and MCT4. b. Western blotting of Pfkfb3, Glut1, c-Myc and Mct4 in HLE and HLF cells infected with lentivirus pmiR-Ctrl or pmiR-192. c. Luciferase activities were measured using reporters with WT or MT miR-192 binding sites of three genes in the 3'-UTR or CDS of luciferase vector. 192positive reporter was used as the positive control. Student t-test was performed. *, p <0.05. d. ECAR was measured in HLF-WT and HLF-192KO cells transfected with 50nM si-Ctrl, si-PFKFB3, si-GLUT1, and si-MYC respectively. e. RT-PCR analysis of five CSC surface markers in HLF-WT and HLF-192KO cells infected with si-Ctrl, si-PFKFB3, si-GLUT1, as well as the

combined si-PFKFB3 and si-GLUT1. UGT2B7 was measured as a negative control. f. FACS analysis of CD24+ and CD44+ populations in HLF-WT cells transfected with si-Ctrl, HLF-192KO cells transfected with si-Ctrl, and HLF-192KO cells transfected with the combined si-PFKFB3 and si-GLUT1.

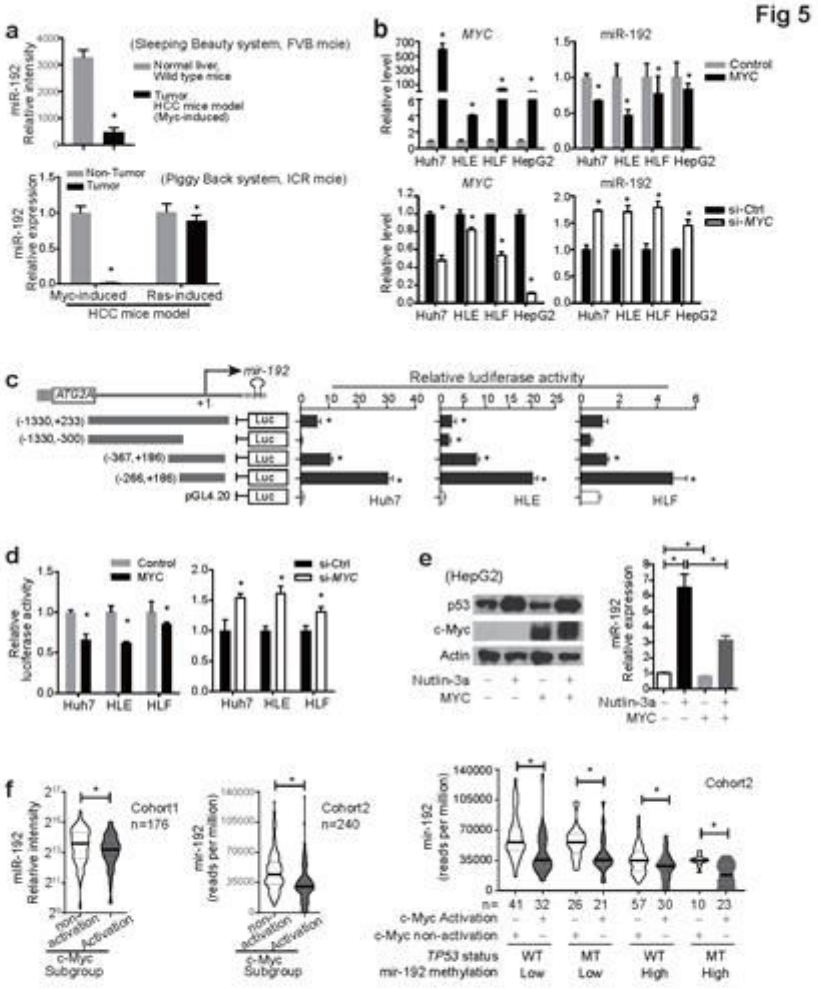

Figure 5

C-Myc activation reduced miR-192 expression in HCC. a. RT-qPCR analysis of miR-192 in oncogene-induced HCC in mice and the corresponding liver controls. RNAs from 3-5 mice for each group were used. b. RT-qPCR analysis of MYC and miR-192 in HCC cell lines (Huh7, HLE, HLF and HepG2) transfected with Ctrl or MYC overexpressing plasmids, as well as with Ctrl or MYC siRNAs, respectively. c. Dual-luciferase assays for different miR-192 promoter fragments in HLE, HLF and HuH7 cells. d. The dual-luciferase assay using miR-192 promoter (-266nt, +186nt) in HLE, HLF and HuH7 cells transfected with Ctrl or MYC

overexpressing plasmids, as well as with Ctrl or MYC siRNAs, respectively. e. Western blotting analysis for p53 and c-Myc, and RT-qPCR analysis for miR-192 in HepG2 treated with Nutlin-3a (10uM) and/or transfected with MYC. f. miR-192 expression levels were shown in c-Myc activation group and c-Myc non-activation group defined in Supplementary Fig. S5c-d in two Cohorts. In Cohort 2, mir-192 expression levels were further shown in subgroups with different status of p53 mutation, mir-192 promoter methylation and c-Myc activation. Student t-test was performed. *, p<0.05.

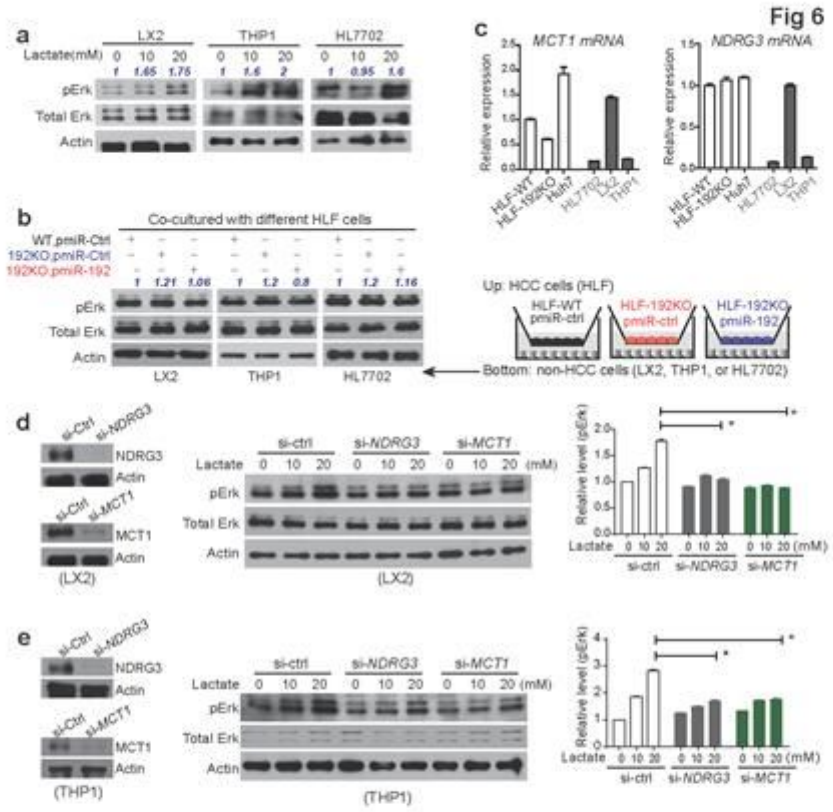

Figure 6

Overproduced lactate from HCC cells with miR-192 loss activated Erk pathway in HCC environmental cells. a. Western blotting analysis for pErk and total Erk in LX2, THP1 and HL7702 cells treated with 0, 10, 20mM lactate. b. Western blotting analysis for pErk and total Erk in LX2, THP1 and HL7702 cells, when

they were co-cultured with HLF-WT and -192KO cells infected with lentivirus pmiR-Ctrl or pmiR-192 in a co-culture chamber system, which showed a schematic in the right panel. c. RT-qPCR analysis of MCT1 and NDRG3 in different HCC and non-HCC cell lines. d. Western blot analysis of pErk and total Erk in LX2 cells transfected with si-NDRG3 or si-MCT1 and treated with different doses of Lactate. e. Western blot analysis of pErk and total Erk in THP1 cells transfected with si-NDRG3 or si-MCT1 and treated with different doses of Lactate. Student t-test was performed. *, p<0.05.

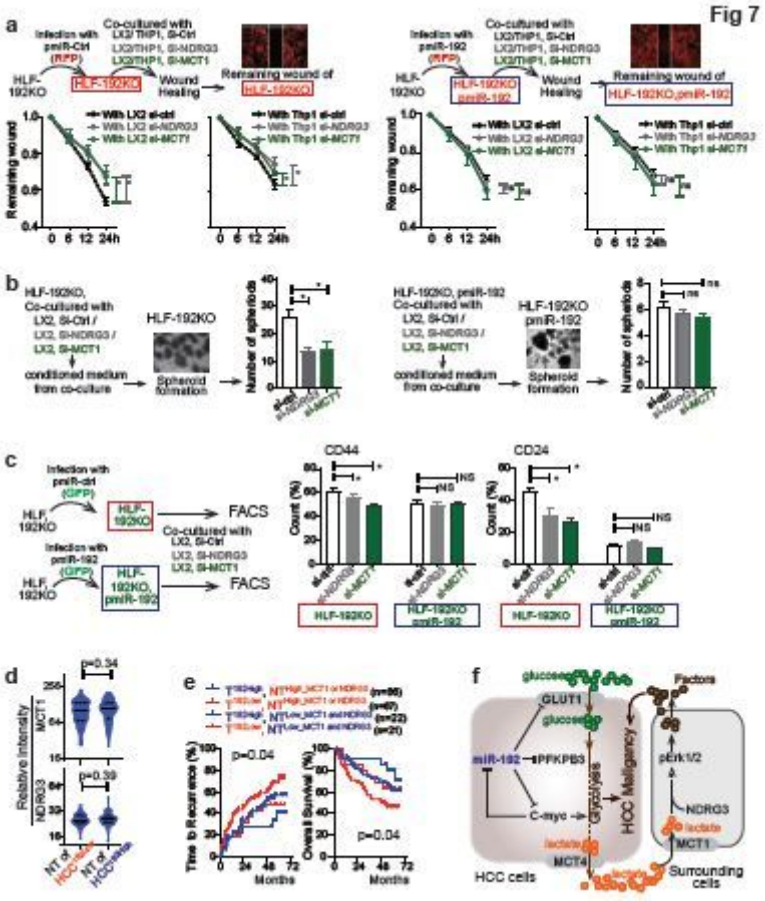

Figure 7

Silencing MCT1 and NDRG3 in LX2 or THP1 cells reduced malignancy and stemness features of co-cultured HCC cells. a. For wound healing assay, scratches were generated in a confluent monolayer HLF cells infected with pmiR-ctrl/RFP or pmiR-192/RFP which were co-cultured with LX2 or THP1 pre-transfected with si-NDRG3 or si-MCT1. b. HLF-192KO cells or HLF-192KO infected with p-miR-192/GFP were used for spheroid formation assay. Conditioned medium was used for this assay and collected from corresponding HLF cells co-cultured with LX2 pre-transfected with si-NDRG3 or si-MCT1. c. Quantitative data of FACS analysis of CD24+ and CD44+ populations in HLF-192KO cells or HLF-192KO infected with p-miR-192/GFP cells co-cultured with LX2 pre-transfected with si-NDRG3 or si-MCT1.Student t-test was used. *, p<0.05. d. Relative levels of MCT1 and NDRG3 in non-tumor samples from patients with different levels of miR-192 in their tumors. e. Kaplan–Meier curves of overall survival and time to recurrence in Cohort 1 according to miR-192 level in tumors as well as MCT1 or NDRG3 levels in non-tumors. f. The schematic model of the miR-192 regulatory pathway in glycolysis and hepatic CSC features.

Supplementary Files

This is a list of supplementary files associated with this preprint. Click to download.

- miR192manuscriptSup.docx